

# Extended Version of GTGraffiti: Spray Painting Graffiti Art from Human Painting Motions with a Cable Driven Parallel Robot

Gerry Chen, Sereym Baek, Juan-Diego Florez, Wanli Qian, Sang-won Leigh, Seth Hutchinson, and Frank Dellaert

**Abstract**—We present a system that paints graffiti art with applications in art preservation, human-robot collaboration, and other tasks which require large-scale dynamic motion. The problem of painting graffiti in a human style is particularly challenging and requires a systems approach because the art and robotics must be designed around each other. Our approach consists of three stages: artwork capture, robot hardware, and robot planning and control. We use motion capture to capture collaborator painting motions which are then composed and processed into a time-varying linear feedback controller for a cable-driven parallel robot (CDPR) to execute. In this work, we will describe the capturing process, the design and construction of a purpose-built CDPR, and the software for turning an artist’s vision into control commands. While we acknowledge that further work is needed for a system which can perfectly recreate human artwork, our results represent a contribution by demonstrating that we can reproduce artist motions up to 2m/s and 10m/s<sup>2</sup> within 2cm to paint artworks.

## I. INTRODUCTION AND RELATED WORK

Spray painting graffiti art in a human style is an important, open problem that requires a systems approach. In this paper, we take the first step towards creating a system that can capture human graffiti artwork and collaborate with artists to create new and copied artworks in the public settings that define graffiti. In addition to the well-established, sociological motivations for reproducing graffiti art [1], robot art is intrinsically motivating for its marriage of art and technology. By possessing physical abilities beyond those of its collaborating artists, a graffiti robot could reveal new artistic avenues highlighting human-robot collaboration for disabled [2] and able-bodied artists alike. To act as the hand of an artist poses inherently interconnected problems in art, hardware, control, and human-robot interaction. Furthermore, the technology required to produce the large-scale, dynamic motions required for graffiti has applications in warehouse/industrial logistics, agriculture [3], construction [4], [5], and motion simulation [6]. Creating graffiti art with a robot requires (1) capturing the motions of artists painting, (2) creating a robot that can achieve comparable motions to human artists, and (3) implementing algorithms that would allow the robot to execute on the artists’ visions. Despite considerable and diverse progress in each of these tasks, to our knowledge, no system has been demonstrated to achieve all three.

This work was supported by the NSF under Grant No. 2008302  
Institute for Robotics and Intelligent Machines, College of Computing,  
Georgia Institute of Technology, Atlanta, GA, {gchen328, ???, ???, wqian39,  
seth, fd27}@gatech.edu



Fig. 1. Artwork of the letters “ATL” (Atlanta) produced by the GTGraffiti system.

Prior work exists in capturing graffiti art, most notably those associated with the Graffiti Markup Language (GML) project. Although the project has been successful in generating a large library of graffiti artwork, almost all the data was captured on digital interfaces (e.g. touchscreen) rather than the real motions of artists. This lack of representation of real motions is problematic because an artist’s creative process may differ between virtual and physical mediums and because ignoring the physical painting motions neglects the challenge of generating robot trajectories. A notable exception is the GML Recording Machine, though it captures only two degree of freedom (DoF) planar motion.

Robots developed for spray painting have seen considerably more attention. Serial arm manipulators and gantry-based systems are precise and mature, but arms do not scale well to large workspaces [7], [8] and gantry-based systems exhibit a tradeoff between size and portability [9], [10]. Mobile manipulators address these issues, but are currently not as dynamic or precise as human artists [11]. Aerial robots are popular for their ability to paint otherwise inaccessible walls, but have been cited as being difficult to accurately control due to susceptibility to disturbances and comparatively limited acceleration capabilities [12]–[15]. Cable-based systems currently appear to be the most promising designs, but so far [2], [16] have only demonstrated raster- or stippling- style painting while [17] has not demonstrated the highly dynamic motions employed by human artists.

Furthermore, despite prior research in robot control and artistic composition separately, the software to enable graffiti painting does not currently exist. CDPR control (further discussed in Section IV-A.3) is relatively well understood, but requires an input trajectory. Research on industrial painting robots has thoroughly studied paint dispersion and trajectory generation, but is primarily concerned with uniform coats on

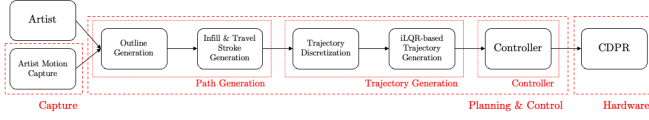


Fig. 2. System overview depicts the capture, hardware, and planning & control components of our system.

curved surfaces in contrast to graffiti art’s non-uniform coats on flat surfaces [18]–[21]. Berio is notable for his research in graffiti composition and stylization [8], [22]–[24], but his work focuses on digital rendering as opposed to producing trajectories.

We argue that the problem of creating graffiti artwork is sufficiently expansive and its components codependent that it requires a systems approach. In this work, we propose a novel system towards creating graffiti artwork by improving and coordinating the capture, hardware, and software requirements. Figure 1 depicts an example result of our system summarized in Figure 2. Our contributions include:

- **capturing** a library of 6 DoF trajectories for creating graffiti artwork using mocap,
- designing, building, and testing the **hardware** for a purpose-made robot platform to paint graffiti,
- proposing a **planning and control** pipeline to realize high-level artistic descriptions into motor torque commands, and
- demonstrating a system that can paint human-style graffiti artwork.

## II. CAPTURE

We describe how we capture painting motions, preprocess the data, and use it to inform robot hardware requirements. In this work, we collect a library of simple shapes which can be composed.

### A. Design Considerations

We first capture artwork using an OptiTrack™ mocap system for its simplicity and accuracy. Mocap systems have the advantage of directly outputting positions and orientations of rigid bodies with sub-millimeter accuracy which trivializes the process of obtaining the 6D trajectories of a spray paint can during painting. As we will discuss in Section IV, the processing and rendering components of our pipeline can optionally use other forms of captured artwork such as Scalable Vector Graphics (SVG) and GML files in addition to mocap data.

We opt to capture only the outlines of shapes and omit the infills because, according to an artist collaborator, the particular pattern used to fill-in a shape is largely arbitrary and does not possess significant artistic value.

### B. Approach

1) *Data Collection Procedure:* We collected the full 6D trajectories of the spray cans and painting surfaces (plywood sheets) as two graffiti artist collaborators painted various symbols. Four mocap position markers were affixed each



Fig. 3. 4 mocap position markers (gray) affixed to a spray paint can via 3D printed structure (white) to track 6DoF spray can pose.

to the can (as shown in Figure 3) and painting surface to extract the 6DoF poses for each time step at 120Hz. One additional marker was placed on the tip of the artist’s index finger to aid in identifying when the spray can nozzle was depressed. For each art collaborator, the 26 letters of the English alphabet were captured along with special symbols such as punctuation marks and small doodles of the artists’ choices (e.g. skull).

2) *Data Pre-processing:* The motion capture data is given in arbitrary “world” coordinates so we must convert the data into the painting surface’s reference frame. The top left (y-axis), bottom left (origin), and bottom right (x-axis) markers of the painting surface are used to obtain the coordinate frame,  ${}_wT_s[k]$ , of the surface in the world frame for each timestep,  $k$ , using Gram-Schmidt Orthogonalization for  $x$  then  $y$ , then using the cross product to obtain the  $z$ -axis. Anecdotally, we found that the fourth mocap marker was never needed, though it would be useful in the event of one of the other three markers missing data. For the spray can, a similar process is performed to obtain the can’s frame,  ${}_wT_c[k]$ . The pose of the spray can’s nozzle in the spray can’s frame,  ${}_cT_n$ , is obtained by manually measuring the position in the spray can’s coordinate system and assigning the identity rotation. Finally, the nozzle’s pose in the painting surface’s frame at timestep  $k$ ,  ${}_sT_n[k]$ , can be expressed as

$${}_sT_n[k] = ({}_wT_s^{-1}[k]) ({}_wT_c[k]) ({}_cT_n)$$

To determine when the spray nozzle is being depressed (painting vs traveling motions), we compute the position of the finger marker in the nozzle’s frame and apply a threshold  $y$ -value. We then manually review and repair any incorrect classifications.

3) *Informing Robot Hardware Requirements:* As an additional analysis, we also study the speeds and accelerations reached by our collaborating artists during painting and traveling to inform the necessary capabilities of the cable robot hardware.

### C. Results

Figure 4a shows an example 2D representation of our data by projecting the can position onto the painting surface, with painting vs traveling denoted as blue and red respectively. We believe the fact that the data was collected while the artists were physically painting combined with the accuracy of motion capture make our data uniquely valuable.

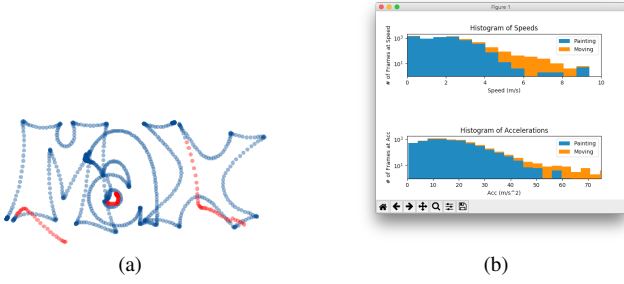


Fig. 4. Plot of painting motion of the name "Max" from motion capture data, — Speeds and accelerations typical of a human graffiti artist which define design constraints of the cable robot

The speeds and accelerations reached by the human graffiti artists is shown in Figure 4b. Based on this, we estimate that a speed of 6m/s and acceleration of 50m/s<sup>2</sup> should be sufficient for a robot to reproduce human graffiti artwork.

#### D. Discussion & Limitations

Although motion capture's accuracy is unparalleled, there are several drawbacks. Most notably, its cost and setup hinder the accessibility and mobility of capture systems. We were only able to capture motions in a controlled laboratory setting which limits the realism of the artwork. The ability to capture nozzle actuation was also limited since we were unable to directly record actuation force which artists use to allow better paint control. Furthermore, manual annotation was needed to correct misclassifications in nozzle actuation. Finally, human artists can move so fast that, even at 120Hz, the mocap system may be missing some detail.

The comprehensiveness of our current dataset is limited, having only captured 58 shape outlines from two artists. We also omitted photographs of the captured artworks. Additional tags, characters, and full murals together with the photographs can be added to the library in the future.

### III. ROBOT HARDWARE

The design constraints for painting graffiti based on real spray painting data will dictate (a) that a CDPR is an ideal choice of hardware platform, and (b) the design of the CDPR.

#### A. Design Considerations

The primary design requirements for a graffiti painting system center around workspace size, maximum end-effector velocity, and maximum end-effector acceleration. We seek a platform which can be easily scaled to 20+ meters square or larger, though in this work we only seek a demonstration sized at a few meters. Based on the analysis of mocap data presented in Section II-C, we determined that we require 6 m/s and 50 m/s<sup>2</sup> of speed and acceleration, respectively. Assuming the mass of the spray can and requisite actuating accessories do not exceed 2kg and compensating for gravity, this means the robot should be capable of exerting 120N upward and 80N downward on the spray can.

Secondary design requirements include portability, accuracy, and stiffness. It should be feasible to deconstruct

and reconstruct the robot on-site at the wall of a building. Accuracy and stiffness are considered secondary constraints because, compared to art forms such as brush painting or sculpture, graffiti is less sensitive to positional inaccuracies and experiences less reaction force. Based on the thickness of a line painted with a "needle" nozzle 5cm from the painting surface, we estimate 2.5cm of repeatability to be sufficient. We estimate an accuracy of 1% the size of the painting to be sufficient, based loosely on [25]. Based on negligible spray paint reaction force and typical wind speeds in Atlanta of 4.1m/s, we estimate external disturbances to be less than 3.1N assuming stagnation pressure applied to a 0.3m<sup>2</sup> end-effector.

CDPR present ideal platforms for graffiti painting given the aforementioned requirements. A CDPR is a robot whose end-effector is pulled by a (redundant) set of cables which are driven by winches on a fixed base. Thanks to properties of cables, CDPRs can scale to extraordinary sizes and speeds [26], [27], with the limitation of reduced stiffness to external wrenches. These qualities make them ideally suited to the large but relatively undisturbed setting and modest accuracy requirement of graffiti painting.

CDPR also have an active research community which has solved many challenges facing CDPRs. Extensive studies in the late 2000's of CDPR workspace analysis [28]–[30] allow designing CDPR with appropriate workspaces. Meanwhile, developments in CDPR control and estimation allow real-time control of CDPR, which will be further discussed in Subsection IV-A.3. Preliminarily, based on [31], we estimate a 1kHz update frequency to be necessary for real-time control.

Finally, we define the requirements to actuate the spray can nozzle. For a full can of Montana BLACK 400mL, the force required to depress the nozzle at the start and end of the stroke was measured to be 20N and 27N, respectively. The displacement was measured to be 2mm. Other 400mL spray cans by the brands Montana, Hardcore, and Kobra were used and found to have similar actuation forces and displacements.

#### B. Approach

1) *CDPR Design:* Our CDPR consists of 4 cables in a planar configuration that can exert pulling forces on the end effector (which carries the spray can) via 4 motor-driven winches. The cable mounting positions on the carriage and routing pulley locations are given in Table I.

The frame is constructed from standard 12 gauge steel strut channel to dimensions 3.05m x 2.44m x 0.61m. The four winches are 2.54cm in diameter with 1.5mm pitch helical grooves to drive 1mm Dyneema® (ultra-high molecular weight polyethylene) rope. They are driven by 150kW D6374 motors from ODrive Robotics and controlled by two ODrive v3.6 56V motor drives. The motor drives are connected via separate, isolated CANbuses to a Teensy 4.0 microcontroller (MCU) running at 600MHz which runs the primary CDPR control, sending torque commands and receiving angular position and velocity feedback to/from the motor drives. The MCU also sends binary spray commands to the spray



TABLE I  
CDPR CABLE CONFIGURATION

Cable Index	End-effector Mounting Location (m)	Routing Pulley Location (m)
1	[0.094, -0.061, 0]	[1.52, -1.22, 0]
2	[0.094, 0.061, 0]	[1.52, 1.22, 0]
3	[-0.094, 0.061, 0]	[-1.52, 1.22, 0]
4	[-0.094, -0.061, 0]	[-1.52, -1.22, 0]

can actuator wirelessly with an HC-05 bluetooth module. The MCU is programmed with the closed-loop controller described in Section IV-A.3.

2) *End Effector Design*: The end effector was built from laser cut 5mm hardwood to carry the spray can and actuating electronics. It consists of the six faces of a box plus two perpendicular midplanes parallel to the gravity vector to center the spray can. The 4 cables are mounted onto the midplane parallel to the painting surface via 1/4"-20 bolts.

3) *Spray Can Nozzle Actuator Design*: The spray can nozzle actuating mechanism is battery-powered and implemented using a "20kg" servo with the lever-arm mechanism from [32]. It is commanded wirelessly.

### C. Results

1) *CDPR As-Built*: The resulting robot is pictured in Figures 1 and 5. The motors are theoretically capable of 600 rad/s and 3.86Nm, which corresponds to 7.62m/s and 94.5m/s<sup>2</sup> for the 2.54cm diameter winch, the 1.96e-4 kgm<sup>2</sup> motor inertia, and a 2kg end-effector mass. Thus the designed motor and winch configuration satisfies our design requirements. The communication **via CANbus between the MCU and motor drives** was measured to have a feedback-command round-trip latency of 626μs and easily achieves the required 1kHz update frequency.

2) *End Effector As-Built*: The end-effector is pictured in Figure 5. The mass of the empty end-effector was measured to be 496g, the battery for the nozzle actuator was 231g, the remaining nozzle actuator components totalled 166g, and the spray can varied from 113g to 424g depending on the fullness, brand, and part-to-part variability. Thus the total mass varied between 1006g and 1317g (within our 2kg assumption).

3) *Spray Can Nozzle Actuator As-Built*: The spray can actuating mechanism is pictured in Figure 5 and was able to successfully depress the spray nozzle 100% of the time in a trial of 100, 1 second long actuations. The delay between the command to actuate the nozzle and the dispensing of paint was measured to be 400ms.

### D. Discussion & Limitations

- 1) 6DoF
- 2) motor cogging
- 3) friction
- 4) distance to canvas
- 5) portability (2 winches per motor controller)

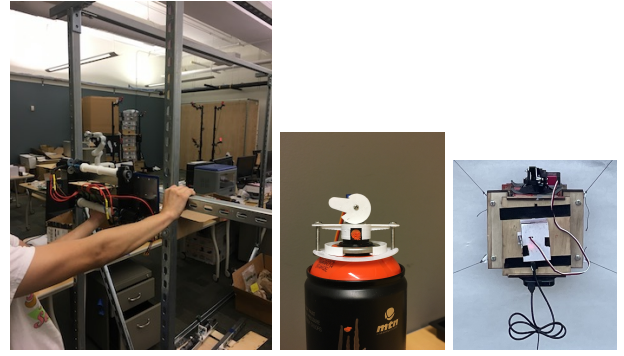


Fig. 5. Cable robot winch assemblies (top) each consist of a motor controller (shared), motor, and helical winch. Spray paint actuator (left) uses a servo to depress the spray can nozzle. End effector (right) carries the spray paint and actuator electronics.

## IV. PLANNING AND CONTROL

From a high-level artistic description, we must control the robot to paint. We use a hierarchical approach with 3 levels:

- 1) Path Generation: turn the artist's vision into a mathematical description
- 2) Trajectory Generation: find a trajectory within the robot's capabilities while respecting the artist's vision to the maximum extent possible
- 3) CDPR Control: online execution of the trajectory

The interplay between the trajectory generation and CDPR control merits a summarized precursor explanation for clarity. During the trajectory generation phase, the optimal control problem of tracking a desired trajectory will be solved *offline*. The iLQR method [33] – iterating by applying the linearized system and control law forward in time and obtaining a new linearized feedback law – is used to solve the optimal control problem. The feedback law from the final pass can then be used as the online controller.

### A. Design Considerations

1) *Path Generation*: At the highest level, given an artist's specification for *poses, sizes, and overlaps rules of shapes* from the library of captured art, we must generate the *paths*, in the form of Bézier curves, required to paint the artwork. This inherently requires a systems-level approach because it depends on the data contained in the shape library, the capabilities of the robot, and the artist's desires. We divide path generation into (1) outline, primarily a human-robot interaction problem, (2) infill, a coverage path planning problem, and (3) travel, a problem of filling in discontinuities. The latter two are unique to our system approach because, recalling the reasoning from Section II, only outlines are captured for the shape library.

2) *Trajectory Generation*: To create a physically realizable trajectory that is as similar as possible to the artist's vision, we first discretize the path at 100Hz to obtain a direct-from-artist trajectory,  $x_d$  (within speed and acceleration limits), then apply an offline iLQR-based optimization to obtain a smoothed reference trajectory,  $x_{ff}$ , control signal,  $u_{ff}$ , time-varying feedback gains,  $K$ , and paint timing.

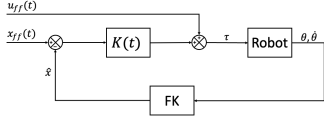


Fig. 6. CDPR controller block diagram, where  $u_{ff}$ ,  $x_{ff}$ , and  $K$  are pre-computed offline using an iLQR-based optimizer implemented in GTSAM.

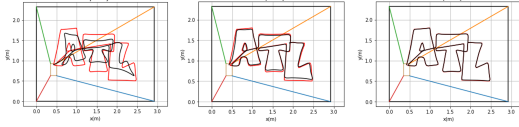


Fig. 7. Stylization from iLQR Q vs R also observed by [23]

Loosely inspired by [23], the iLQR-based optimization is used to strike a balance between the artist’s intent and the ease of controlling the robot. We express the iLQR *problem* in discretized form with time index  $k$  as:

$$\begin{aligned} \mathbf{x}_{ff}, \mathbf{u}_{ff} &= \arg \min_{\mathbf{x}, \mathbf{u}} \sum_{k=0}^T \tilde{\mathbf{x}}[k]^T Q \tilde{\mathbf{x}}[k] + \tilde{\mathbf{u}}[k]^T R \tilde{\mathbf{u}}[k] \quad (1a) \\ \text{s.t.} \quad & \mathbf{x}[k+1] = f(\mathbf{x}[k], \mathbf{u}[k]), \quad (1b) \\ & \mathbf{x}[0] = \mathbf{x}_0 \quad (1c) \end{aligned}$$

where  $\tilde{\mathbf{x}}[k] := \mathbf{x}[k] - \mathbf{x}_d[k]$  is the deviation of the state  $\mathbf{x}[k]$  from  $\mathbf{x}_d[k]$ : the artist’s intended trajectory,  $\tilde{\mathbf{u}}[k] = \mathbf{u}[k] - \mathbf{u}_m$  is the deviation of the control  $\mathbf{u}[k]$  from  $\mathbf{u}_m$ : the average of the minimum and maximum allowable torques [34], [35],  $\mathbf{x}_{ff}$  and  $\mathbf{u}_{ff}$  are the reference nominal (feedforward) state and control signals,  $Q$  and  $R$  are the state objective and control cost matrices,  $f(\mathbf{x}[k], \mathbf{u}[k])$  defines the nonlinear system dynamics, and  $\mathbf{x}_0$  is the initial state. The state consists of the cartesian position and velocity:  $\mathbf{x} = [p_x \ p_y \ \dot{p}_x \ \dot{p}_y]$ , where  $\mathbf{p}$  denotes the position of the spray can’s nozzle. The control  $\mathbf{u}$  consists of the four motor torques. Section IV-C experimentally justifies why orientation is omitted.

Intuitively, the state objective matrix,  $Q$ , advocates for the artist and the control cost matrix,  $R$ , penalizes being near torque limits. Interestingly, as discovered by [23], the relationship between  $Q$  and  $R$  can also be interpreted as an artistic parameter as visually depicted in Figure 7.

3) *Control*: We seek a controller that can control the cable robot to achieve motions comparable to a graffiti artist. Similarly to Section III-A, we require maximum speed of 7 m/s, maximum acceleration of 50 m/s<sup>2</sup>, repeatability of 2.5cm, accuracy of 1% the size of the painting, and external disturbance rejection ability of 3.1N.

Our cable robot controller is heavily inspired by prior works. CDPR control places emphasis on “tension distribution” (TD) which is, loosely speaking, an analogue to redundancy resolution in serial manipulators [6], [31], [34], [36]–[40]. These approaches typically use or assume a feedback controller whose control variable is a task space wrench. The TD algorithm then computes the optimal motor torques (corresponding to cable tensions) required to achieve the desired task space wrench.

However, since we are using an iLQR-based optimizer, which produces locally optimal control laws as described in Section IV-A.2, most aspects of control (including TD) have been shifted offline. Our online controller is then a simple linear feedback controller. Figure 6 depicts a block diagram of our controller. Mathematically, our controller can be expressed as

$$\boldsymbol{\tau} = K(t)(\mathbf{x}_{ff}(t) - \hat{\mathbf{x}}) + \mathbf{u}_{ff}(t) \quad (2)$$

where  $\boldsymbol{\tau}$  is the 4-vector of motor torques,  $\hat{\mathbf{x}}$  is the measured state, and  $K(t)$  is the 4x4 time-varying gain matrix.

To compute  $\hat{\mathbf{x}}$ , we need to estimate the position and velocity of the spray can well enough to achieve our repeatability and accuracy requirements. Although a nonlinear least squares solver is typically used to estimate position for CDPR, we seek a simpler solution due to concerns over guaranteed convergence, speed, and ease of implementation.

## B. Approach

1) *Path Generation*: To generate the outline, the most challenging part is communicating the artist’s intent and robot’s capabilities between the artist and computer which inherently requires a systems-level approach. In this work, we apply constraints to the artist when they are specifying their artistic vision. To constrain the canvas size, we use a rectangular approximation of the wrench feasible workspace (WFW) [29], [30] to define the space in which the artist may place library objects. To constrain layering specifications, we impose a strict layering of library objects such that each library object is either entirely on top of or entirely beneath another. Due to our robot’s planar limitation, we project the nozzle position for each frame from the library data onto the painting surface to form an ordered set of 2D line segments (allowing us to retain velocity information to be used during trajectory generation). Data sources other than our mocap library can be used but require velocity data.

To infill the shapes we apply a horizontal lawn-mower pattern. Similarly to the way each artist chooses a strategy for infilling based on what is easiest for him or her (according to our artist collaborators), we choose this pattern for its ease of implementation and actuation: in most configurations our robot has the best control authority horizontally. Further details on the way we split up and order cells in the lawn-mower pattern to reduce nozzle actuation cycles are provided in our accompanying arXiv paper. We paint the infill for each object in the face color then the outline in the outline color. **This is in contrast to human artists who typically start with the outline in the face color, proceed to fill it in, then re-assert the outline in the outline color. The initial face color outline is usually for visual reference and our system does not have such imagination constraints so we opt to omit the initial face color outline.** Instead of applying a hidden line removal algorithm, we simply finish painting each object before the next is started.

Finally, travel strokes must be added to make the path continuous in position. Although making the paths continuous in direction is another option (as in [17]), we opt instead

to allow discontinuous directions but enforce continuous velocity in the trajectory generation stage. For every pair of strokes, we simply add a straight line connecting the end of the previous stroke with the start of the next stroke if they are not already coinciding.

2) *Trajectory Generation*: Unique to the system-level approach, we discretize outlines and infill/travel strokes differently due to the different ways the paths were generated.

For outlines, we have velocities from mocap data so we need to apply time-scaling. We compute the original path's speed and acceleration using finite differences assuming each line segment takes 1s, then apply the linear transformation,  $t' = ct$ , to match a predefined maximum speed and/or maximum acceleration and sample  $x(t')$  from the path at 100Hz. We choose limits of 2.0m/s and 20m/s<sup>2</sup> based on the spray paint dispersion described further in Section IV-C.

For the infills and travel strokes, we need to generate rest-to-rest trajectories from scratch with continuous velocities. We choose trapezoidal velocity profiles for their popularity in industrial applications [41] with limits of 0.5m/s and 20m/s<sup>2</sup> again based on spray paint dispersion.

The iLQR-based optimization of (1) is performed offline using factor graphs and the GTSAM software library, but any iLQR implementation can be used. The system dynamics constraints (1b) are drawn from prior works in CDP control including the standard equations for kinematics and cable tension/wrench equilibrium [34], winch model dynamics [31], [39], rigid body dynamics [39], and numerical integration [42], [43]. The iLQR problem is then expressed using the factor graph [44]–[46] shown in Figure 8 and solved with the GTSAM software library using the Levenberg-Marquardt algorithm and variable elimination. The solution gives  $x_{ff}$  and  $u_{ff}$ , while the Bayes Net obtained by the final iteration's elimination step contains the locally optimal feedback gain matrix,  $K$ . Full details of the equations and factor graph elimination can be found in our accompanying arXiv paper.

To solve using the iLQR-based solver, we do include the orientation using  $T$  is the SE(2) pose,  $\mathcal{V}$  is the twist, and  $\dot{\mathcal{V}}$  is the twist acceleration.  $x$  corresponds to the translational component of  $T$  and, when representing  $T$ ,  $\mathcal{V}$ , or  $\dot{\mathcal{V}}$  as vectors, we use the convention that the orientation is the first element and the translation the latter two. The iLQR problem is expressed as the factor graph in Figure 8. Due to space constraints, we refer the reader to [44]–[46] for an introduction to factor graphs and how they can be applied to optimal control, respectively. The equations for each of the factors is given in Table IV-B.2. For the elimination order, we eliminate timesteps in the order  $K, K-1, \dots, 1$  and, within each timestep, eliminate variables in the order  $l, \dot{l}, \ddot{l}, t, \dot{\mathcal{V}}, \tau, \mathcal{F}, \mathcal{V}, T$  (the order of cable index subscripts  $i$  is arbitrarily chosen to be ascending). The nonlinear factor graph is optimized (equivalent to solving with the iLQR method [46]) to obtain  $x_{ff}$  and  $u_{ff}$ . The graph is then linearized using the optimized solution as the linearization point and eliminated one final time to obtain a Bayes Net. From the resulting Bayes Net, for each timestep we obtain

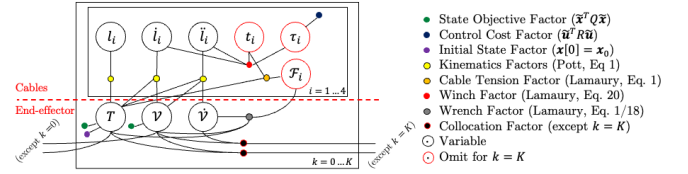


Fig. 8. Factor graph depicting the iLQR problem using plate notation. Circles represent variables to be solved while dots represent objectives or equations.  $l_i$ ,  $\dot{l}_i$ , and  $\ddot{l}_i$  represent cable length, speed, and acceleration respectively.  $t_i$ ,  $\tau_i$ , and  $\mathcal{F}_i$  represent cable tension, motor torque, and the wrench on the end-effector caused by cable  $i$ , respectively.  $T$ ,  $\mathcal{V}$ , and  $\dot{\mathcal{V}}$  represent end-effector pose, twist, and twist-acceleration, respectively.

TABLE II  
EQUATIONS FOR THE FACTORS IN FIGURE 8

Factor Name	Factor Equation/Expression
Winch	$\tau_i = (t_i r - \mathcal{T} \ddot{l}_i / r + f(l_i, \dot{l}_i) r)$
Cable Tension	$\mathcal{F}_i = t [b_i \times \hat{r}_i, \hat{r}_i]$
Kinematics	$l_i = \ \mathbf{r}_i\ _2$ $\dot{l}_i = ([\text{Ad}_{[0; -b_i]}] \mathcal{V}) \cdot [0; \hat{r}_i]$ $\ddot{l}_i = ([\text{Ad}_{[0; -b_i]}] \dot{\mathcal{V}}) \cdot [0; \hat{r}_i]$
Wrench	$\sum_i [\text{Ad}_{[0; b_i]}]^T \mathcal{F}_i + m g = \mathcal{G} \dot{\mathcal{V}} - [\text{ad}_{\mathcal{V}}]^T \mathcal{G} \mathcal{V}$
Control Cost	$\ \tau_i - (\tau_{min} + \tau_{max})/2\ _{R^{-1/2}}^2$
State Objective	$\ T - T_d\ _{Q^{-1/2}}^2$
Initial State	$T[1] = T_0$ $\mathcal{V}[1] = \mathcal{V}_0$
Collocation	$T[k+1] = T[k] + dt \mathcal{V}[k]$ $\mathcal{V}[k+1] = \mathcal{V}[k] + dt \dot{\mathcal{V}}[k]$

where  $f(l, \dot{l}) = -(\mu \tanh(50\dot{l}) + b\dot{l})$  is the friction,  $\mathbf{r}_i = T b_i - \mathbf{a}_i$  is the vector from the routing pulley location  $\mathbf{a}_i$  to the end effector mounting point ( $b_i$  in the end-effector frame),  $\hat{r}_i = \frac{\mathbf{r}_i}{\|\mathbf{r}_i\|}$  is the normalized  $\mathbf{r}_i$ ,  $\text{Ad}_T$  is the Adjoint of the transformation  $T$  [47],  $\mathcal{G}$  is the inertia matrix,  $\text{ad}_{\mathcal{V}}$  is the adjoint of the twist  $\mathcal{V}$ ,  $\tau_{min}$  and  $\tau_{max}$  are the minimum and maximum allowable torques respectively (based on [34]),  $R$  is the control cost matrix from iLQR,  $Q$  is the state objective cost matrix from iLQR,  $T_d$  is the desired pose,  $T_0$  and  $\mathcal{V}_0$  are the initial pose and twist respectively, and  $dt$  is the time step duration. The second-order effects for the cable acceleration kinematics were assumed to be negligible. Superscripts ( $k$ ) are omitted for TODO: for what?

(among other equations):

$$\Delta \tau^*(\Delta \mathcal{F}, \Delta \mathcal{V}, \Delta T) = K_{\tau, \mathcal{F}} \Delta \mathcal{F} + K_{\tau, \mathcal{V}} \Delta \mathcal{V} + K_{\tau, T} \Delta T$$

$$\Delta \mathcal{F}^*(\Delta \mathcal{V}, \Delta T) = K_{\mathcal{F}, \mathcal{V}} \Delta \mathcal{V} + K_{\mathcal{F}, T} \Delta T$$

where  $\cdot^*$  denotes the optimal value. By substituting  $\mathcal{F}^*(\Delta \mathcal{V}, \Delta T)$ , we can now obtain the control law and gain matrix  $K$  for each timestep:

$$\tau^*(\Delta \mathcal{V}, \Delta T) = \Delta \tau^*(\Delta \mathcal{V}, \Delta T) + u_{ff}$$

$$= (K_{\tau, \mathcal{F}} K_{\mathcal{F}, \mathcal{V}} + K_{\tau, \mathcal{V}}) \Delta \mathcal{V} + (K_{\tau, \mathcal{F}} K_{\mathcal{F}, T} + K_{\tau, T}) \Delta T + u_{ff}$$

$$K = \begin{bmatrix} K_{\tau, \mathcal{F}} K_{\mathcal{F}, \mathcal{V}} + K_{\tau, \mathcal{V}} \\ K_{\tau, \mathcal{F}} K_{\mathcal{F}, T} + K_{\tau, T} \end{bmatrix}$$

3) *Control*: First we interpolate  $K$ ,  $x_{ff}$ , and  $u_{ff}$  since the trajectory generation phase was discretized at 100Hz while the controller runs online at 1kHz.  $K$  and  $u_{ff}$  are interpolated using a zero-order hold, while  $x_{ff}$  is interpo-



Fig. 9. During path generation, we first produce the outline from artist inputs (left), then infill paths (center), and finally travel strokes (right).

lated using a first-order extrapolation from the most recent discrete  $x_{ff}$ .

To estimate position we discard redundant information and to estimate velocity we use a linear least squares solution. We discard the bottom two cable lengths then apply the law of cosines using the top two cable lengths to estimate the spray can position assuming the spray can is always vertical. To estimate velocity, we solve the linear least squares problem:

$$\begin{aligned}\dot{\mathbf{p}} &= \arg \min_{\dot{\mathbf{p}}} \left\| \dot{\mathbf{i}} - \mathbf{W}^T \dot{\mathbf{p}} \right\|_2^2 \\ &= \mathbf{W}^T \dot{\mathbf{i}}\end{aligned}$$

where  $\mathbf{W}$  is the *wrench* matrix (Jacobian transpose) [39] and  $\cdot^+$  denotes the Moore-Penrose left pseudoinverse.

### C. Results

1) *Path Generation*: An example path generation result is shown in Figure 9.

2) *Trajectory Generation*: We qualitatively found the speed and acceleration limits to be reasonable at the intended painting distance of around 12cm. The outline limits of 2.0m/s and 20m/s<sup>2</sup> were tested using the Montana “Skinny Cap Beige” nozzle. The infill limits of 0.5m/s and 20m/s<sup>2</sup> were tested using the Montana “flat jet cap wide” nozzle. Faster speeds resulted in incomplete coverage while slower speeds resulted in “dripping”.

The offline iLQR-based optimization has  $\mathcal{O}(n)$  complexity and runs at approximately half real-time (e.g. a 1-minute trajectory takes 2 minutes to optimize).

3) *Control*: To evaluate our control stage, we use mocap for ground truth data and log the robot’s estimated and setpoint states at 100Hz for the same trajectory as was used for Figure 1. The mocap and robot coordinate frames were aligned using the 4 pulley locations and the mocap data was piecewise cubic interpolated to match the 100Hz robot log frequency.

We show that the can is always close to vertical, our estimation is sufficiently accurate, and our controller can track the desired trajectory well. To validate our assumption the can always close to vertical, which is used both for online control and estimation, we measured the greatest absolute deviation from vertical to be X degrees as evidenced in Figure 11. Figures 10 and 11 show that the position and velocity estimates match the ground truth within Xcm and Xm/s respectively. Finally, Figures 10 and 11 show that the controller can maintain a state within Xcm and Xm/s of the desired trajectory. We believe our proposed controller, which precomputes linear feedback gains offline, is easier

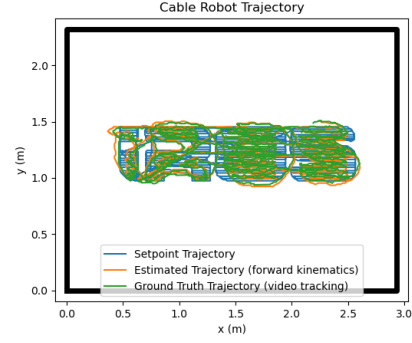


Fig. 10. Setpoint, estimated, and ground truth trajectories of the “IROS” logo as executed by the cable robot graffiti painting system.

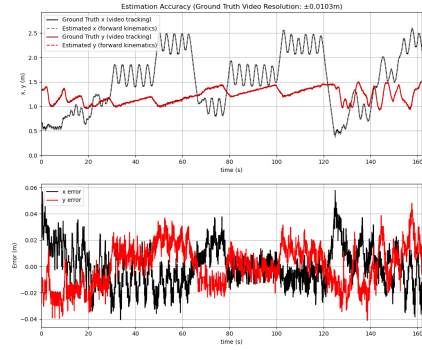


Fig. 11. Ground truth and online estimate of spray can x/y position (top) and error (bottom). The resolution of the ground truth is 10mm

to implement and useful for CDPR applications other than graffiti as well.

In addition to the painting in Figure 1, please refer to our supplemental video for additional painting results which qualitatively demonstrate our system’s capabilities.

### D. Discussion & Limitations

Many of our discoveries in planning and control, both problems we revealed and problems we solved, are difficult to quantify but highly relevant for future research in this direction.

When specifying an artist’s vision, the total space of creative possibilities are simply indescribable. For example, even when constrained to our finite library of shape outlines, the ability specify non-flat overlap topologies [22], homographies, non-linear, and other 3D perspective transforms have artistic interest but are beyond the scope of this work. Graffiti stylization [23] and freeform inputs [48] are beyond the scope of this work. Because in this early work we cannot explore a large descriptive space, we decided to follow the maxim, “Creativity is born from limitation” and begin by constraining the artist to motivate creativity.

Understanding the nuances of paint dispersion is another large area of study that we simply could not tackle in this work. One obvious question that arises is how the human



graffiti artists could consistently paint solid lines at 6m/s while our robot's lines would thin at 2m/s. We believe this to be a limitation of our distance to the canvas, which was 5cm in this work compared to  $3.0\text{cm} \pm 1.3\text{mm}$  by the artist. Additionally, since we only have a 2DoF robot attempting to reproduce 6DoF data, we naively project the nozzle positions onto the painting surface during path outline generation but should instead model how the paint would appear on the canvas. Finally, we neglect stroke width when computing the infill path but should include this. Abundant opportunities exist for further analysis of paint dispersion for artistic effects, e.g. flaring, blending, and intentional dripping.

For our controller, we do find some limitations on the  $Q$  matrix. For large  $Q$  matrices ( $\|Q\|_2 / \|R\|_2 \geq 1e6\text{N/m}$ ), the controller resonates with the natural vibrations described in Section III-D causing damage to the robot while for small  $Q$  matrices ( $\|Q\|_2 / \|R\|_2 \leq 1e2\text{N/m}$ ), the robot gets stuck for a few cm before overcoming the friction and returning to the setpoint trajectory.

Nevertheless, we found that our controller was remarkably well suited for our application. While we had initially attempted using a controller based on [39], we had trouble tuning the parameters and gains to allow the controller to overcome parasitic forces and made the mistake of choosing the minimum norm tension distribution instead of the centroid. Friction and motor cogging were some of the greatest challenges that we faced. Cogging was particularly challenging to overcome because the motors are overpowered compared to the speeds and accelerations that we are running them, which increases the ratio of cogging torque to actuation torque. We found that minimizing  $\|u - u_m\|$  instead of  $\|u\|$  (maximizing the torque limit margin) significantly improves controller performance and is easier to implement than the centroid calculation in [31]. Compared to [34], [35], we believe the iLQR method is marginally easier because it requires less tuning. Although our linearized control law does not explicitly solve the inequality constrained TD problem that is standard in the literature, we find that most times the torque is not saturated and simply clamping the torque to its limits as needed is sufficient. Finally, we found a control frequency on the order of 1kHz to be necessary, having been unable to achieve motions faster than 0.5m/s with a 250Hz control frequency.

## V. CONCLUSIONS & FUTURE WORK

We demonstrated a system for successfully recreating graffiti art. Our system contributes to existing research in capturing artwork, building a graffiti robot, and planning and controlling a graffiti robot for painting graffiti. Our work can be applied to graffiti preservation by recreating captured artwork, human-robot collaboration in art by enhancing the physical capabilities of artists, and other fields through technology transfer for large-scale dynamic motion.

Avenues for future work include a more portable graffiti capture device, better communication of robot workspace limits to the artist, style analysis and improvisation, paint

dispersion analysis, real-time human-robot interaction, an enlarged workspace, and 6 DoF motion by the CDPR.

## ACKNOWLEDGEMENTS

We thank Max and Jules for collaborating as graffiti artists, Prajwal Vedula and Zhangqi Luo for contributing to code, and Russel Gentry, Jake Thompkins, and Tristan Al-Haddad at Georgia Tech's Digital Fabrication Lab for their hardware assistance and allowing us to use their space for painting. NSF ?

## REFERENCES

- [1] L. MacDowall, "In praise of 70k: Cultural heritage and graffiti style," *Continuum*, vol. 20, no. 4, pp. 471–484, 2006.
- [2] A. Liekens, Kenny, and L. Scheire, "Zet kenny binnenkort zélf zijn eerste graffiti op een muur? — team scheire #9 [will kenny soon put his first graffiti on a wall? — team scheire #9]," <https://youtu.be/jOpgvW7alhQ>, Sept 2020.
- [3] J. M. Pagan, "Cable-suspended robot system with real time kinematics gps position correction for algae harvesting," Ph.D. dissertation, Ohio University, 2018.
- [4] F. Shahmiri and R. Gentry, "A survey of cable-suspended parallel robots and their applications in architecture and construction," *Blucher Design Proceedings*, vol. 3, no. 1, pp. 914 – 920, 2016.
- [5] R. Bostelman, J. Albus, N. Dagalakis, A. Jacoff, and J. Gross, "Applications of the nist robocrane," in *Proceedings of the 5th International Symposium on Robotics and Manufacturing*, vol. 5, 1994.
- [6] P. Miermeister, M. Lächele, R. Boss, C. Masone, C. Schenk, J. Tesch, M. Kerger, H. Teufel, A. Pott, and H. H. Bühlhoff, "The cablerobot simulator large scale motion platform based on cable robot technology," in *2016 IEEE/RSJ International Conference on Intelligent Robots and Systems (IROS)*, 2016, pp. 3024–3029.
- [7] L. Scalera, E. Mazzon, P. Gallina, and A. Gasparetto, "Airbrush robotic painting system: Experimental validation of a colour spray model," in *Advances in Service and Industrial Robotics*, C. Ferraresi and G. Quaglia, Eds. Cham: Springer International Publishing, 2018, pp. 549–556.
- [8] D. Berio, S. Calinon, and F. F. Leymarie, "Learning dynamic graffiti strokes with a compliant robot," in *IEEE/RSJ Intl. Conf. on Intelligent Robots and Systems (IROS)*. IEEE, 2016, pp. 3981–3986.
- [9] L. Scalera, S. Seriani, A. Gasparetto, and P. Gallina, "Watercolour robotic painting: a novel automatic system for artistic rendering," *Journal of Intelligent and Robotic Systems*, pp. 1–16, 2018.
- [10] N. Roy, "Graffiti robot - train writing - planet256 / niklas roy / the fly - wall printer style machine," [https://www.youtube.com/watch?v=zSIdvQsu27s&t=3s&ab\\_channel=ARTESANOBERLIN](https://www.youtube.com/watch?v=zSIdvQsu27s&t=3s&ab_channel=ARTESANOBERLIN).
- [11] Y. Jun, G. Jang, B.-K. Cho, J. Trubatch, I. Kim, S.-D. Seo, and P. Y. Oh, "A humanoid doing an artistic work - graffiti on the wall," *2016 IEEE/RSJ International Conference on Intelligent Robots and Systems (IROS)*, pp. 1538–1543, 2016.
- [12] A. Uryasheva, M. Kulbeda, N. Rodichenko, and D. Tsetserukou, "Dronegraffiti: Autonomous multi-uav spray painting," in *ACM SIGGRAPH 2019 Studio*, ser. SIGGRAPH '19. New York, NY, USA: Association for Computing Machinery, 2019. [Online]. Available: <https://doi.org/10.1145/3306306.3328000>
- [13] A. S. Vempati, M. Kamel, N. Stilinovic, Q. Zhang, D. Reusser, I. Sa, J. Nieto, R. Siegwart, and P. Beardsley, "Paintcopter: An autonomous uav for spray painting on three-dimensional surfaces," *IEEE Robotics and Automation Letters*, vol. 3, no. 4, pp. 2862–2869, 2018.
- [14] B. Galea, E. Kia, N. Aird, and P. G. Kry, "Stippling with aerial robots," in *Computational Aesthetics (Expressive 2016)*, 2016, p. 10 pages.
- [15] TsaruRobotics, "Autonomous mural for sprite ukraine," <https://tsuru.su/en/project/spritemural/>. [Online]. Available: <https://tsuru.su/en/project/spritemural/>
- [16] "Albert robot muralist," <https://www.robotmuralist.com/albert>. [Online]. Available: <https://www.robotmuralist.com/albert>
- [17] J. Lehn, "Soft monsters," *Perspecta*, vol. 40, pp. 22–27, 2008. [Online]. Available: <http://www.jstor.org/stable/40482274>



- [18] Y. Chen, W. Chen, B. Li, G. Zhang, and W. Zhang, "Paint thickness simulation for painting robot trajectory planning: a review," *Industrial Robot: An International Journal*, vol. 44, no. 5, pp. 629–638, 2021/09/04 2017. [Online]. Available: <https://doi.org/10.1108/IR-07-2016-0205>
- [19] H. Chen, T. Fuhlbrigge, and X. Li, "A review of cad-based robot path planning for spray painting," *Industrial Robot: An International Journal*, vol. 36, no. 1, pp. 45–50, 2021/09/04 2009. [Online]. Available: <https://doi.org/10.1108/01439910910924666>
- [20] M. V. Andulkar, S. S. Chiddarwar, and A. S. Marathe, "Novel integrated offline trajectory generation approach for robot assisted spray painting operation," *Journal of Manufacturing Systems*, vol. 37, pp. 201–216, 2015. [Online]. Available: <https://www.sciencedirect.com/science/article/pii/S0278612515000229>
- [21] Y. Zeng, J. Gong, N. Xu, and N. Wu, "Tool trajectory optimization of spray painting robot for manytimes spray painting," *International Journal of Control and Automation*, vol. 7, pp. 193–208, 08 2014.
- [22] D. Berio, P. Asente, J. Echevarria, and F. F. Leymarie, "Sketching and layering graffiti primitives," in *8th ACM/Eurographics Expressive Symposium, Expressive 2019, Genoa, Italy, May 5-6, 2019, Proceedings*, C. S. Kaplan, A. G. Forbes, and S. DiVerdi, Eds. Eurographics Association, 2019, pp. 51–59. [Online]. Available: <https://doi.org/10.2312/exp.20191076>
- [23] D. Berio, S. Calinon, and F. F. Leymarie, "Dynamic graffiti stylisation with stochastic optimal control," in *Proceedings of the 4th International Conference on Movement Computing*. ACM, 2017, p. 18.
- [24] D. Berio and F. F. Leymarie, "Computational models for the analysis and synthesis of graffiti tag strokes," in *Proceedings of the Workshop on Computational Aesthetics*. Eurographics Association, 2015, pp. 35–47.
- [25] L. DELLA VALLE, T. G. ANDREWS, and S. ROSS, "Perceptual thresholds of curvilinearity and angularity as functions of line length," *J Exp Psychol*, vol. 51, no. 5, pp. 343–347, May 1956.
- [26] R. Nan, D. Li, C. Jin, Q. Wang, L. Zhu, W. Zhu, H. Zhang, Y. Yue, and L. Qian, "The five-hundred-meter aperture spherical radio telescope (fast) project," *International Journal of Modern Physics D*, vol. 20, no. 06, pp. 989–1024, 2011.
- [27] S. Bandyopadhyay, "Lunar crater radio telescope (LCRT) on the far-side of the moon," <https://www.nasa.gov/directorates/spacetech/niac/2020%5FPhase%5FI%5FPhase%5FI%5FPhase%5FI%5Fcrater%5Fradio%5Ftelescope/>, April 2020.
- [28] P. Bosscher, A. T. Riechel, and I. Ebert-Uphoff, "Wrench-feasible workspace generation for cable-driven robots," *IEEE Transactions on Robotics*, vol. 22, no. 5, pp. 890–902, 2006.
- [29] S. Bouchard, C. Gosselin, and B. Moore, "On the ability of a cable-driven robot to generate a prescribed set of wrenches," *Journal of Mechanisms and Robotics*, vol. 2, no. 1, 2/15/2021 2009.
- [30] M. Gouttefarde, D. Daney, and J. Merlet, "Interval-analysis-based determination of the wrench-feasible workspace of parallel cable-driven robots," *IEEE Transactions on Robotics*, vol. 27, no. 1, pp. 1–13, 2011.
- [31] M. Gouttefarde, J. Lamaury, C. Reichert, and T. Bruckmann, "A versatile tension distribution algorithm for  $n$ -dof parallel robots driven by  $n + 2$  cables," *IEEE Transactions on Robotics*, vol. 31, no. 6, pp. 1444–1457, 2015.
- [32] A. Liekens, "Spray can servo mount," <https://www.thingiverse.com/thing:4622176>, Oct 2020.
- [33] E. Todorov and W. Li, "A generalized iterative lqg method for locally-optimal feedback control of constrained nonlinear stochastic systems," in *Proceedings of the 2005, American Control Conference, 2005.*, 2005, pp. 300–306.
- [34] A. Pott, T. Bruckmann, and L. Mikelsons, "Closed-form force distribution for parallel wire robots," in *Computational Kinematics*, A. Kecskeméthy and A. Müller, Eds. Berlin, Heidelberg: Springer Berlin Heidelberg, 2009, pp. 25–34.
- [35] P. Miermeister, A. Pott, and A. Verl, "Auto-calibration method for overconstrained cable-driven parallel robots," in *ROBOTIK 2012; 7th German Conference on Robotics*, 2012, pp. 1–6.
- [36] M. Agahi and L. Notash, "Redundancy resolution of wire-actuated parallel manipulators," *Transactions of the Canadian Society for Mechanical Engineering*, vol. 33, no. 4, pp. 561–573, 2009.
- [37] M. Hassan and A. Khajepour, "Analysis of bounded cable tensions in cable-actuated parallel manipulators," *IEEE Transactions on Robotics*, vol. 27, no. 5, pp. 891–900, 2011.
- [38] H. D. Taghirad and Y. B. Bedoustani, "An analytic-iterative redundancy resolution scheme for cable-driven redundant parallel manipulators," *IEEE Transactions on Robotics*, vol. 27, no. 6, pp. 1137–1143, 2011.
- [39] J. Lamaury and M. Gouttefarde, "Control of a large redundantly actuated cable-suspended parallel robot," in *2013 IEEE International Conference on Robotics and Automation*, 2013, pp. 4659–4664.
- [40] W. Shang, B. Zhang, S. Cong, and Y. Lou, "Dual-space adaptive synchronization control of redundantly-actuated cable-driven parallel robots," *Mechanism and Machine Theory*, vol. 152, p. 103954, 2020. [Online]. Available: <https://www.sciencedirect.com/science/article/pii/S0094114X20301750>
- [41] B. Siciliano, L. Sciacivico, L. Villani, and G. Oriolo, *Robotics: modelling, planning and control*. Springer Science & Business Media, 2010, ch. 4.
- [42] D. Lau, J. Eden, Y. Tan, and D. Oetomo, "CASPR: A comprehensive cable-robot analysis and simulation platform for the research of cable-driven parallel robots," in *IEEE/RSJ International Conference on Intelligent Robots and Systems (IROS)*. IEEE, 2016.
- [43] *Numerical Differential Equation Methods*. John Wiley & Sons, Ltd, 2016, ch. 2, pp. 55–142. [Online]. Available: <https://onlinelibrary.wiley.com/doi/abs/10.1002/9781119121534.ch2>
- [44] F. Dellaert and M. Kaess, "Factor graphs for robot perception," *Foundations and Trends in Robotics*, vol. 6, pp. 1–139, 2017.
- [45] S. Yang, G. Chen, Y. Zhang, F. Dellaert, and H. Choset, "Equality constrained linear optimal control with factor graphs," in *2021 IEEE International Conference on Robotics and Automation (ICRA)*, 2021.
- [46] G. Chen and Y. Zhang, "LQR control using factor graphs," <https://gtsam.org/2019/11/07/lqr-control.html>, Nov 2019, note: Superseding ICRA 2021 paper pending review.
- [47] K. Lynch and F. Park, *Modern Robotics: Mechanics, Planning, and Control*. Cambridge University Press, 2017.
- [48] D. Berio, F. F. Leymarie, and R. Plamondon, "Expressive curve editing with the sigma lognormal model."